
Learning Genomic Structure from k -mers

Filip Thor*

Division of Scientific Computing,
Department of Information Technology
Science for Life Laboratory
Uppsala University
Uppsala SE-752 37, Sweden
filip.thor@it.uu.se

Carl Nettelblad

Division of Scientific Computing,
Department of Information Technology
Science for Life Laboratory
Uppsala University
Uppsala SE-752 37, Sweden
carl.nettelblad@it.uu.se

Abstract

Sequencing a genome to determine an individual's DNA produces an enormous number of short nucleotide subsequences known as reads, which must be reassembled to reconstruct the full genome. We present a method for analyzing this type of data using contrastive learning, in which an encoder model is trained to produce embeddings that cluster together sequences from the same genomic region. The sequential nature of genomic regions is preserved in the form of trajectories through this embedding space. Trained solely to reflect the structure of the genome, the resulting model provides a general representation of k -mer sequences, suitable for a range of downstream tasks involving read data. We apply our framework to learn the structure of the *E. coli* genome, and demonstrate its use in simulated ancient DNA (aDNA) read mapping and identification of structural variations. Furthermore, we illustrate the potential of using this type of model for metagenomic species identification. We show how incorporating a domain-specific noise model can enhance embedding robustness, and how a supervised contrastive learning setting can be adopted when a linear reference genome is available, by introducing a distance thresholding parameter Γ . The model can also be trained fully self-supervised on read data, enabling analysis without the need to construct a full genome assembly using specialized algorithms. Small prediction heads based on a pre-trained embedding are shown to perform on par with BWA-aln, the current gold standard approach for aDNA mapping, in terms of accuracy and runtime for short genomes. Given the method's favorable scaling properties with respect to total genome size, inference using our approach is highly promising for metagenomic applications and for mapping to genomes comparable in size to the human genome. In both scenarios, the flexibility of not being tied to a single linear reference can provide a more nuanced analysis of input data.

1 Introduction

Modern next-generation sequencing (NGS) platforms generate massive numbers of short subsequences of DNA referred to as *reads*, which consist of sequences of nucleotide bases *A*, *T*, *C* and *G* [1]. Reads contain no inherent positional information. Therefore, reconstructing the full genome of an individual from reads requires reassembling them, which is typically done by aligning them to the most similar region in a reference genome – a process known as *read mapping* or *read alignment* [2]. Performing a unique read alignment proves challenging when there are repetitive or highly similar segments in the genome. When reads are shorter, ambiguities become more prevalent [3]. One of the leading short read sequencing platforms, Illumina, produces reads that can vary from 30 to 500

*Corresponding author

base pairs (bp) [4], but recent developments in DNA sequencing have made long read sequencing more reliable and available, producing reads of lengths 10k to 100k bp [5]. This greatly facilitates alignment, as most regions are unique at those length scales. In this work, we analyze sequences 30bp in length, which would represent read lengths that can occur in ancient DNA (aDNA) sequencing [6]. aDNA is characterized by specific damage patterns, such as cytosine deamination that increases individual nucleotide errors, and also suffers from severe fragmentation [7]. Fragmentation of genetic material prevents the recovery of longer reads, regardless of advancements in sequencing technology. Thus, robust methods for analyzing ultra-short read data are still needed for us to learn about our past through studying genetics.

Our contribution. We introduce a framework we have named Contrastive Read Network (CRead-Net). Inspired by recent developments in contrastive representation learning, we demonstrate how an encoder model can be trained to map short k -mers (a sequence of k nucleotides) to a general embedding reflecting the genomic structure. This is done by extracting two k -mers with a small genetic distance (measured in bps), minimizing their distance in the embedding space, and maximizing the distance to other k -mers. Due to transitivity, this yields a continuous embedding that reflects the ordering of the k -mers within the genome. Depending on the data available, we frame the problem in either a supervised or self-supervised contrastive learning setting. This training is task-agnostic, producing a general representation that can be used for a diverse set of tasks. We demonstrate how a pre-trained encoder model can be used to identify both structural variation in a genome and discriminate between disjoint sequences. The latter has a potential for applications in metagenomics. In our experiments, we focus on aDNA read mapping. For this task, we show that a model predicting the bitwise representation of the read position outperforms a regression model of equal size. We also show that using a small GPT to sequentially predict bits improves the accuracy further.

The framework is illustrated in Figure 1. Our main contributions can be summarized in three points:

- We apply contrastive learning to train a neural network that learns a continuous representation of a genome based on short k -mers, or sequences of base pairs.
- We demonstrate how a domain-adapted augmentation scheme makes the model robust to intricacies found specifically in genetic read data.
- We frame the read mapping problem as a classification problem on a bitwise representation of the coordinate, improving over regression, and scaling better than predicting equidistant bins.

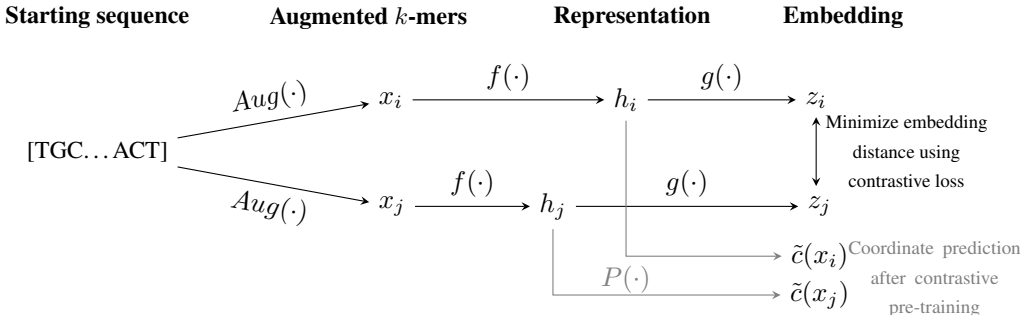


Figure 1: Given a starting sequence, we draw two k -mers, $Aug(\cdot)$ adds aDNA noise, resulting in pairwise positive k -mers x_i and x_j . A convolutional encoder model f and a one-layer projection layer g are trained to minimize the embedding distances between z_i and z_j . The intermediate representation h_i is used by a prediction head P when predicting k -mer coordinates c_i .

Related work. There has been some work in genome alignment using deep learning approaches. BetaAlign [8] uses transformers to do multi-sequence alignment, matching groups of 10 reads with each other. Similarly, Lall and Tallur [9] does pairwise read alignment using reinforcement learning and focuses on developing models tailored for edge devices. Millán Arias et al. [10] uses unsupervised learning to cluster long reads (~ 10 kbp). Busia et al. [11] uses a convolution-based NN to do species identification from short reads. Shrestha [12] does short read genome alignment. In contrast to our

work, their model treat alignment as a single multi-class classification problem, binning the reference genome into several classes, and predicting the approximate position of a given read. Our work demonstrates how a pre-trained meaningful general representation of the DNA structure can be used for several applications, not only read mapping, and we show how to target the difficulties arising when analyzing aDNA reads specifically.

2 Methodology

The core principle in contrastive learning is simple: each sample in a batch gets designated *positive* and *negative* samples, and a neural network is trained using a loss that attracts the positives, and repulses the negatives [13–15]. In this work, we adapt this methodology and apply it to genetic read data. We aim to create an embedding of k -mers that reflects the genomic structure, which can be used for downstream tasks involving short-read data. Following the workflow in Figure 1, we start by introducing the data and the augmentation scheme, followed by our customized loss function and the neural network models used.

k -mers, Directionality, and Read Complements. We consider k -mers, substrings k nucleotide bases in length extracted from some longer sequence. For example, the sequence [TGCGTGG] has the following 3-, 4- and 5-mers

$$[TGCGTGG] \rightarrow \begin{cases} \text{3-mers: } \{[TGC], [GCG], [CGT], [GTG], [TGG]\}, \\ \text{4-mers: } \{[TGCG], [GCGT], [CGTG], [GTGG]\}, \\ \text{5-mers: } \{[TGCGT], [GCGTG], [CGTGG]\}. \end{cases}$$

DNA sequences are double-stranded, and in short-read genome sequencing, one does not know which strand of the double helix the sequence comes from. This means that a read can be expressed in terms of its *reverse complement*, i.e., in reversed order and with the bases changed as $A \leftrightarrow T$ and $C \leftrightarrow G$ when compared to the reference genome, which describes just one of the strands. Figure 2 illustrates an excerpt of the double helix, and shows that reads from the same genomic position can be expressed differently depending on which strand the read is taken from. To handle real short-read data, the model must recognize a k -mer and its reverse complement as similar.

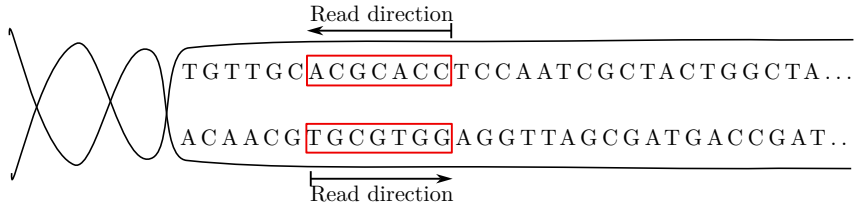


Figure 2: Reads from the same position in the genome can be expressed differently based on which strand the sequence originates from, [TGCGTGG] and [CCACGCA] have the same bp coordinate.

We use a one-hot encoding of the input k -mer as input to our encoder model. By choosing the base ordering A, C, G, T , the reverse complement is obtained by simply flipping both axes in one-hot encoded data, as shown in Equation (1).

$$\text{RevComp}([TGCGTGG]) = \text{RevComp} \left(\begin{pmatrix} 0 & 0 & 0 & 1 \\ 0 & 0 & 1 & 0 \\ 0 & 1 & 0 & 0 \\ 0 & 0 & 1 & 0 \\ 0 & 0 & 0 & 1 \\ 0 & 0 & 1 & 0 \\ 0 & 0 & 1 & 0 \end{pmatrix} \right) = \begin{pmatrix} 0 & 1 & 0 & 0 \\ 0 & 1 & 0 & 0 \\ 1 & 0 & 0 & 0 \\ 0 & 1 & 0 & 0 \\ 0 & 0 & 1 & 0 \\ 0 & 1 & 0 & 0 \\ 1 & 0 & 0 & 0 \end{pmatrix} = [CCACGCA] \tag{1}$$

Sequencing Errors and aDNA Damage. In NGS, many types of errors can contaminate the produced reads. The most common error types are substitutions, where one base is substituted by another, and indels, where a base can either be deleted or inserted between two bases. Here, we try

to mimic Illumina sequencing, where substitutions are the most common, and have a prevalence of 0.1–1% [16]. We want to apply our method to aDNA, which has additional characteristic damage patterns. Aged DNA samples have drastically reduced fragment length, shortening the read length. They also suffer from deamination damage, a chemical process that breaks down the cytosine base. This is expressed as a higher error rate for the $C \rightarrow T$ and $G \rightarrow A$ substitutions close to the ends of the reads [7]. We want the model to be robust to both the read complement and the types of noise we expect to see in real aDNA data.

Augmentation Scheme. In contrastive learning, we train a model to minimize distances between *similar* samples. The augmentation scheme applied to the positives is important, since we then implicitly state that two augmented versions of a sample are still supposed to be considered to be *similar*. Ideally, the augmentation should cover the kinds of deviations from the non-augmented training data that can be expected during inference. We want to train the model to attract two k -mers if they **1**: have a small distance in the genome, **2**: are reverse complements of each other, and **3**: are noisy versions of the same k -mer. An embedding that satisfies these three conditions captures the genomic structure faithfully. Combining these three attributes, we use the following augmentation scheme $Aug(\cdot)$. Given a starting sequence of length L , and a maximum offset between positive k -mers d , we sample the starting coordinate of the first k -mer x_i as $c_i \sim \mathcal{U}(0, L - k - d)$, and the coordinate of its positive x_j as $c_j \sim \mathcal{U}(c_i, c_i + d)$. With a probability of 0.5, we apply the reverse complement transformation separately for all k -mers, and add a flat 1% substitution rate in all positions. We restrict ourselves to considering k -mers of length 30 to be able to handle the short read lengths in aDNA, and to model the deamination noise, we increase the substitution rate for $C \rightarrow T$ in the first 10 bases and $G \rightarrow A$ in the last 10 bases to 10%. The starting sequence will be the reference genome if available, otherwise, the pair of positive k -mers will be drawn from the same read of larger total length.

Coordinate-Thresholded Contrastive Loss. We train the model using an altered version of the simCLR loss, which can be used in a supervised as well as a purely self-supervised contrastive learning setting. We use the following definition for the loss function, following the notation in [17]

$$\mathcal{L} = \sum_{i \in I} \frac{-1}{|P(i)|} \sum_{p \in P(i)} d_{i,p} \log \frac{\exp(z_i \cdot z_p / \tau)}{\sum_{a \in A(i)} \exp(z_i \cdot z_a / \tau)}, \quad (2)$$

where z_i are the k -mer embeddings produced by the model, τ is a temperature parameter, $I = \{1, \dots, 2N\}$ the set of all indices in a batch, and $A(i) = \{I \setminus i\}$ and $P(i)$ the set of negatives and positives of k -mer i , respectively. In self-supervised learning, the positive is just the positive pair from the augmentation, $P(i) = j$. When we have access to a reference genome and thus know the coordinates c_i used in training, we can extend the set of positives to include all nearby k -mers by introducing a thresholding parameter Γ , and define the positives as

$$P(i) = \begin{cases} \{p \in I \mid |c_i - c_p| \leq \Gamma\}, & \text{if supervised} \\ j, & \text{if self-supervised.} \end{cases} \quad (3)$$

This choice has two main benefits. We increase the number of positives, which has been shown to positively impact performance [17]. When using large batches and large augmentation offsets d , it will be common for a supposed negative to be closer to the anchor than the positive. This means that the gradients would have repulsion terms from samples that are genomically closer than the assigned positive. Γ -thresholding makes those samples positives, instead. If the augmentation offset $d < \Gamma$, we are guaranteed to always have at least one positive per sample. In the worst case the supervised loss collapses to the self-supervised formulation. We also introduce a distance scaling in the thresholded loss, which weights the loss contributions by the distance between the anchor and each positive, defined as $d_{i,p} = \frac{|c_i - c_p|}{\Gamma}$, which in the self-supervised setting is just set to 1.

Encoder Model Architecture. We use a ConvNet as the encoder network since we want a translationally invariant model that captures local patterns within the k -mers. We adopt a similar residual block and overall structure as the ConvNeXt model by Liu et al. [18], with some alterations tailored toward short DNA sequences. Since the reads are very short, we use stride 1 in the input stem, and use regular rather than depthwise convolutions. The residual block structure is shown in Figure 3. After each stage of residual blocks, the input is downsampled using an average pooling with stride 2 and kernel size 2, followed by a convolution with kernel size 3, doubling the channels.

We use the same compute ratio as ConvNeXt with four compute stages, and we scale the model as:

- CReadNet-T: Channels = (64, 128, 256, 512), Blocks = (3, 3, 9, 3), 16.8M params,
- CReadNet-S: Channels = (64, 128, 256, 512), Blocks = (3, 3, 27, 3), 29.8M params,
- CReadNet-B: Channels = (96, 192, 384, 768), Blocks = (3, 3, 27, 3), 66.5M params.

The encoder model ends with global average pooling and a dense layer with the same number of units as the output channels pre-pooling, which produces the representation h_i . A last linear layer then outputs the 256-dimensional embeddings z_i . Both z_i and h_i are L_2 normalized.

Position Prediction. The main application we target is read alignment, which means finding the position of a read along a reference genome. Here, we define the coordinate of a k -mer as the position of its first nucleotide. Analogous to classification heads used in image classification, we employ a smaller network $P(\cdot)$ to perform the mapping task. This model is trained using the representation h_i , with the encoder model weights frozen. We compare three different ways of doing this, all starting with a 3-layer MLP with 2,048 units, using layer normalization before, and SiLU activation after, in each layer. The first approach is using a regression model, where the output of the MLP is the predicted coordinate $\tilde{c}(x)$, and the model is trained using the MSE loss, $L_{MSE} = \sum_{i=0}^N |c_i - \tilde{c}(x_i)|^2$.

The other alternatives use a classification approach. A natural option would be to split the reference genome into B sized bins, and train a model to predict the probability that a read falls into each bin, as in [12]. This approach can be effective for small genomes or when large bins are acceptable, but leads to either large bins (reducing precision) or a huge number of bins (increasing complexity) for large genomes. We therefore explore alternate strategies that should better scale to larger genomes. Inspired by works like Chen et al. [19], we convert coordinates c into the one-hot encoding of their bitwise representation $c_b = [t_1, t_2, \dots, t_{N_b}]$, where $t_n \in \{0 \dots b-1\}$ and $N_b = \lfloor \log_b(L) \rfloor + 1$. For example, the coordinate $c = 20000$ would in base 2 be expressed as

$$20000_2 = \begin{bmatrix} 0 & 1 & 1 & 0 & 0 & 0 & 1 & 1 & 1 & 0 & 1 & 1 & 1 & 1 & 1 \\ 1 & 0 & 0 & 1 & 1 & 1 & 0 & 0 & 0 & 1 & 0 & 0 & 0 & 0 & 0 \end{bmatrix}.$$

We then train a classifier to predict each bit in this sequence by outputting softmaxed probabilities for each element, using the categorical cross-entropy loss. This reformulates the task from a single classification problem with L/B classes into N_b classification problems with b classes, yielding a logarithmic rather than linear scaling of the output dimension, decreasing the problem size for large genomes.

In the above model, all bits are predicted independently, and it does not utilize the fact that the value of a more significant bit would influence the interpretation, and hence the predictions, of subsequent bits. To incorporate this information, the last approach we introduce is a bit-predicting GPT model. We employ a lightweight GPT that follows the standard transformer architecture [20], consisting of causally masked multi-head self-attention, layer normalization, and a feed-forward network. The model uses just one transformer block, 2 heads, a feed-forward dimension of 256, and a token dimension of 64. We set the output dimension of the MLP to 512, and split it into 8 64-dimensional tokens, which become the starting sequence during inference. We use a trainable embedding for the bit-tokens and add a trainable positional encoding. The model has full attention across the MLP tokens, and each bit prediction uses information from the MLP tokens, *and only* the previously predicted bits, increasing the information used in each prediction. The prediction models are illustrated in Figure 4.

In read alignment, we want to get the exact placement of the reads within the reference, and predicting the exact position proves challenging for any of these methods. If we can predict an approximate position, local alignment can be performed cheaply by sliding the read across a small window near the predicted location and finding the best match. This local alignment can be efficiently parallelized on a GPU, while attempting to do this over the full genome is computationally infeasible. Classical algorithms for alignment, such as BWA, also tend to first identify a seed position and then perform an alignment/extension process around that seed. For short reads, the seed identification process dominates the computational load.

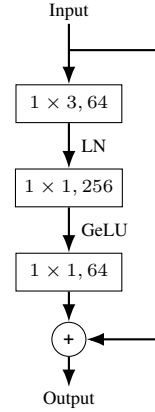


Figure 3: Residual block layout.

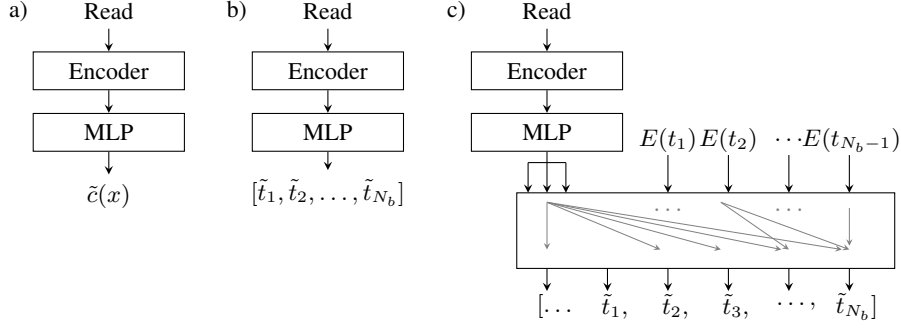


Figure 4: Different prediction heads for the coordinate prediction task. a): An MLP using regression to predict k -mer position $\tilde{c}(x)$. b): MLP predicting the bitwise probabilities using the representation h . c): A small GPT predicting probabilities using h and the previous bits.

Training and Evaluation data. To illustrate the potential of our method, we apply it to learn the structure of the *Escherichia coli* (*E. coli*) genome, accession number NC_000913 [21]. It has 4.64 million nucleotides and is a common model species. In the numerical experiments, we use the reference genome as the starting sequence. We draw k -mers with $k = 30$, and use a maximum positive offset of $d = 50$. When evaluating model performance on unseen data, we create 30bp reads using the Gargammel ancient DNA simulator [22], which simulates Illumina sequencing errors using the ART read simulator [23] and applies aDNA noise using the Briggs model [7].

3 Numerical Experiments

In this section, we evaluate how well the embeddings reflect genomic structure, present the short-read mapping performance, and demonstrate other potential uses of a pre-trained model. When visualizing k -mer embeddings, we take a small excerpt of the genome since the full embeddings are very long trajectories in \mathbb{R}^{256} which are hard to visualize in 2D plots.

Genome Embeddings and Thresholding Parameter. Here we study the effect that the magnitude of Γ has on the embedding. We train the CReadNet-B on the first 10% of the *E. coli* genome, and Figure 5 shows a scatterplot of a 20kbp snippet of the embedding, where each marker is an embedded k -mer, colored by its true bp coordinate. We have taken the normalized 256-dimensional embedding and applied PCA to visualize it in two dimensions. The subpanels of Figure 5 show, from left to right: the embedding using $\Gamma = 1000$, the embedding using $\Gamma = 100$, and a density plot of the mean distance to each embedded k -mer's 10 closest neighbors. Both choices of Γ produce embeddings that preserve the genomic structure, with a trajectory reflecting the ordering of the coordinates of the k -mers, and both have an average bp distance to the 10 closest k -mers less than 100. Γ determines how tightly the reads will be mapped, with a smaller Γ better capturing the local structure, while a larger value gives a less complex manifold, which may simplify downstream tasks.

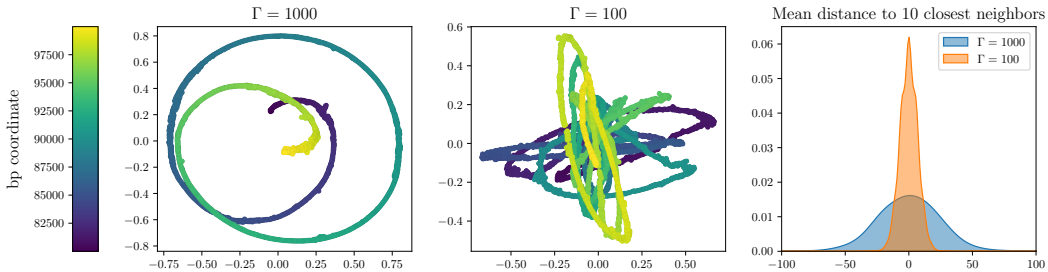


Figure 5: 2D PCA of the resulting embedding over a 20kbp window, with $\Gamma = 1000$ (left) and $\Gamma = 100$ (middle), and the distribution of the mean distance to the 10 closest neighbors for each sample (right).

Better Error Model Improves Performance. Here we show the influence of the augmentation scheme, specifically, which type of noise is applied. Figure 6 shows a 2D PCA plot of the first 10k base pairs using CReadNet-T, trained on 10% of the *E. coli* genome. Across columns, the plots show the augmentation scenarios of no added noise, a flat 1% substitution rate, and the aDNA error noise model, respectively. Across rows, the evaluation data is instead varied, with error-free reads, simulated reads using only sequencing noise, and simulated aDNA reads using Gargammel, respectively. The clean upper triangle shows that a model trained on high noise generalizes well to less noisy data, but not vice versa.

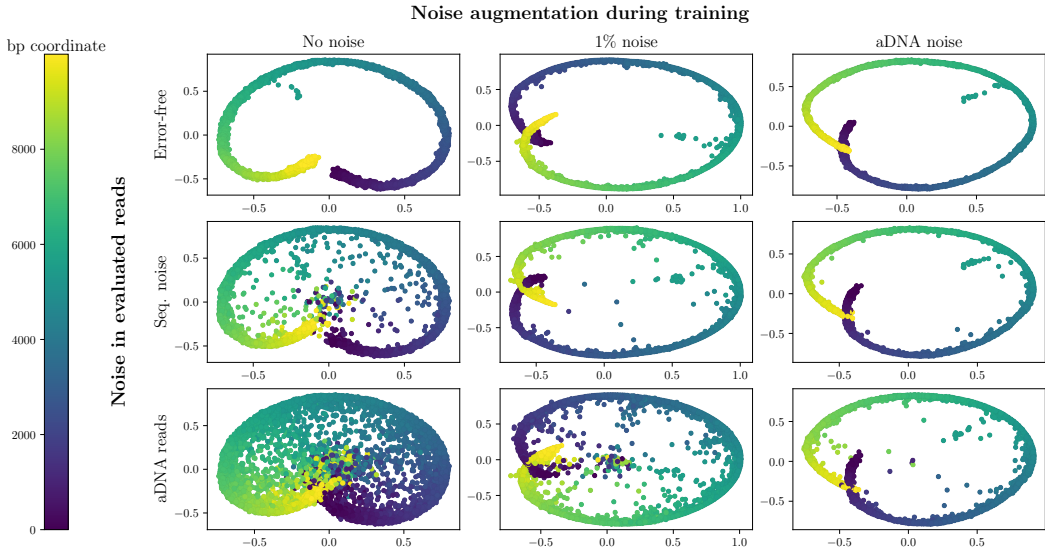


Figure 6: 2D PCA plots of the first 10k base pairs of embeddings, showing the difference in the resulting embedding when training with different augmentation strategies (columns), for varying levels of data corruption (rows).

Read Alignment of aDNA Reads. Given trained embeddings, we train the three read mapping prediction heads for both the first 10% and the full *E. coli* genome, and evaluate the mapping performance on simulated aDNA reads. We denote the regression model *MSE*, the bit prediction model *CCE*, and the GPT model *GPT*, all trained for 10k iterations, and use base 3 in the bitwise representation. The mapping results are shown in Table 1, where we report the percentage of correctly mapped reads after the local alignment step, and the throughput measured in millions of reads processed per second. We compare with BWA-aln, with different values of the maximum edit distance n . The default value, which is also recommended in the literature for aDNA, corresponds to $n = 3$ for 30 bp reads [24]. BWA-mem is usually considered the standard method for short-read alignment, but often underperforms for aDNA [24]. Bowtie2 [25] is another common read aligner, also for aDNA, but we include both as a reference for standard aligners that fail when aligning aDNA reads. For BWA-mem and Bowtie2 we have used the best performing (BP) parameters for aDNA [24, 26]. Reported scores are the medians across 3 different seeds. The scores for each run are shown in the Appendix, as well as plots illustrating the performance without local alignment. The reported throughput for our models is measured by averaging 10 steady-state inference steps. The timings for the local alignment step are omitted. A poorly optimized CuPy [27] implementation we made has a throughput of 0.68 million reads per second on a single A100 when using a 5000bp window, and better optimized approaches should yield negligible overhead.

Inversion Detection and Structural Variation. In addition to substitutions, insertions, and deletions, *inversions* can also occur, where a section of the genome has been replaced by its reverse complement, such as $TGC...GTGG \rightarrow TGAC...GGG$. Such inversions may have a detrimental effect if certain genes are affected. Since the encoder maps short subsequences close to each other, the distance in embedding space between two k -mers from the same longer read should be small. If, however, a pair of k -mers come from different sides of the border of an inversion, we would expect

Table 1: Ancient DNA read mapping score reported as the percentage of correctly mapped reads, along with the throughput of the methods, reported in 10^6 reads/s (MR/s). The mode denotes the number of allowed mismatches for BWA-aln, or the prediction head used. Best practice parameters are used for Bowtie2 and BWA-mem.

Method	10%			100%			100%			100%		
	Mode	Acc.	MR/s	Mode	Acc.	MR/s	Mode	Acc.	MR/s	Mode	Acc.	MR/s
Bowtie2	BP	9.78	0.023	BP	13.14	0.023	-	-	-	-	-	-
BWA-mem	BP	54.76	0.204	BP	54.89	0.181	-	-	-	-	-	-
BWA-aln	$n = 3$	98.02	0.375	$n = 3$	97.08	0.230	-	-	-	-	-	-
BWA-aln	$n = 6$	99.06	0.115	$n = 6$	98.06	0.042	-	-	-	-	-	-
CReadNet-T	CCE	98.71	0.424	CCE	94.19	0.422	GPT	95.26	0.117	MSE	14.40	0.426
CReadNet-S	CCE	98.78	0.232	CCE	95.72	0.229	GPT	96.59	0.095	MSE	21.50	0.231
CReadNet-B	CCE	98.78	0.139	CCE	97.47	0.137	GPT	97.66	0.074	MSE	65.64	0.138

an abnormally large embedding distance. To illustrate how our embedding can be used for inversion detection, we train CReadNet-T on 10% of the *E. coli* reference genome. Then, we create a new reference with inversions 1kbp in length at coordinates 10k, 40k, and 70k, and generate 150bp reads using the ART read simulator [23]. From these reads, we draw two k -mers as the first and last 30 bps, and the pairwise embedding distance is shown in Figure 7. The three inversions stand out, but also another region at around 20kbp. The right-hand subpanels show the distribution of predicted coordinates of the 250 closest embedding neighbors for k -mers predicted to be inside the proposed inversion region. From this, we can infer whether we have a duplication within the genome or a structural variation in the form of an inversion. If we have a multimodal distribution, it is a repeating sequence found at multiple points in the genome, and if it is unimodal, we can conclude it is an inversion.

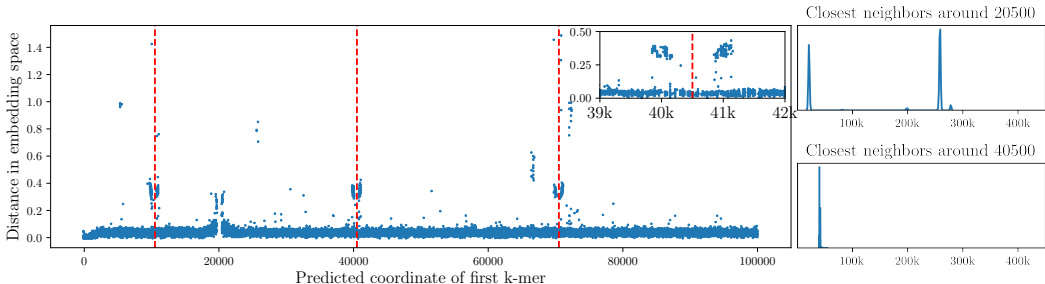


Figure 7: The distance in embedding space between two 30bp k -mers from the same 150bp read, plotted against the predicted coordinate, indicates structural variation. The distances highlight both artificially added inversions (red dashed lines), as well as duplications found in the *E. coli* genome.

Disjoint Sequences and Non-Model Species. There are organisms for which we do not have a reference. In that case, we are unable to use the supervised contrastive framework, but are limited to training on reads only. This is simulated by training solely on pairwise augmented k -mers as positives. The data used in this experiment is two disjoint 10k subsequences of the *E. coli* genome starting at bp 10k and 70k, simulating a case with data from two different organisms. In Figure 8 we show 2D UMAP [28] plots of the embedding $\Gamma = 1000$, $\Gamma = 100$, and the self-supervised loss. In all three cases, we can see that the embedding reflects that the two sequences are disjoint. Clustering k -mers in two groups is trivial. For longer sequences, this methodology can be used for metagenomic species identification. This has been run on a small toy example for ease of visualization as a proof of concept.

4 Conclusions

In this paper, we have introduced a framework for learning the genomic structure from short sequences of DNA called k -mers. Previous literature on using deep learning methods for analyzing DNA data

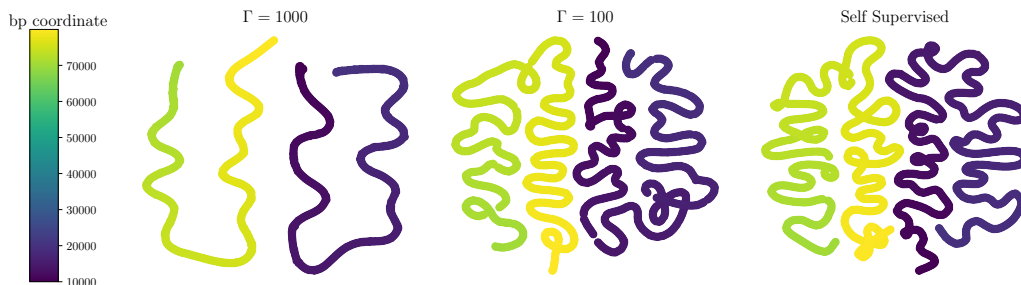


Figure 8: UMAP applied to embedding produced by CReadNet-T trained on two 10kbp excerpts from the *E. coli* genome, using $\Gamma = 100$, $\Gamma = 1000$, and using a self-supervised approach mimicking a case where no reference is available.

has often been developed for a single application in mind, whereas we in this work produce a general representation that can be used for several applications.

We introduce the bitwise prediction of the read coordinates. This approach offers several benefits. A bitwise representation can be thought of as a hierarchical binning approach. In base two, the most significant bit decides in what half of the reference the k -mer should be placed, corresponding to two bins of size $L/2$. Given the first bit, the next bit determines the next halving of the interval, a classification of two bins of size $L/4$, and so on. The bit representation reduces the number of outputs while still allowing for fine-grained predictions. Another advantage over a direct regression output is that the model outputs softmaxed probabilities, giving quantified confidences for each predicted bit. These could be used to make the local alignment step even cheaper by adapting the window size in the local alignment step. Predicting each bit in isolation works surprisingly well, outperforming the regression approach with essentially the same model complexity. We show that the GPT can utilize this and attain even higher accuracy – albeit at a larger inference cost. This approach could be extended to other large-domain prediction tasks to reduce complexity.

Table 1 shows that the prediction models perform on par with the default values for the gold-standard BWA-aln in aDNA mapping. Setting the maximum edit distance to 6 increases the accuracy, but it is not a standard choice in the literature. BWA-aln reports that 3.5% of all reads from the full *E. coli* genome are ambiguous, with multiple hits across the genome. With this in mind, accuracies above 96.5% will only improve by choosing the correct position out of a set of equally good alignments. BWA-aln scales logarithmically with the size of the reference, whereas for a fixed model complexity, inference using our model stays essentially constant. Also, there is performance to be gained by using model quantization and weight pruning, which we have not explored so far.

Thus far, we have considered the reference genome as the ground truth for the genomic structure of a species. That is an idealization that has been common in the field of genomics. However, the established reference genomes can lack genomic regions, including full genes, carried by some individuals within a species. There can also be major structural variations, where the same genes can appear in different distinct orderings. This is an issue for bacterial genomes [29], but it is also of significant importance in the human reference GRCh38, which misses up to millions of base-pairs [30–32]. Since our method can operate without a reference, it can recognize the full genomic complexity, as long as it is present in the training data. In the specific case of aDNA mapping, so-called reference bias [33] is also an important issue. When considering single letter genetic variants (single nucleotide polymorphisms, SNPs), reads that contain the reference allele are successfully mapped more frequently. This may have a detrimental effect on downstream analyses. In our framework, this could be amended by applying SNP-specific augmentation schemes that would ensure that alternate alleles would map just as well as their reference counterparts. For both of these applications, there is also an equity aspect, since many reference resources were originally defined based on privileged populations found in developed nations. Likewise, for studying issues such as antimicrobial resistance, such genes can appear in regions that deviate from the reference sequence.

Future work. Figure 8 demonstrates two possible future applications. Our model produces embeddings of k -mers that distinguish samples coming from two disjoint sequences, simulating a case where we have reads from two different organisms. Here, reads from different organisms, or different

chromosomes or plasmids within an organism, would form distinct trajectories in the embedding, enabling metagenomic species identification based on k -mers. It also shows that self-supervised training could be used for *de novo* assembly, building up the full genome sequence from reads into a trajectory in the embedding space, from which a skeleton graph can be extracted.

Limitations. Currently, we have only trained the model on a bacterial genome. Scaling the model up to e.g. human genomes (from $5 \cdot 10^6$ to $3 \cdot 10^9$ bps) will pose additional challenges. Training the embedding step is highly expensive, compared to building the index for conventional mapping methods, while our approach might be competitive compared to performing a full *de novo* genome assembly. The training cost might be decreased with transfer learning from a pre-trained model to a related genome.

References

- [1] Michael L. Metzker. Sequencing technologies — the next generation. *Nature Reviews Genetics*, 11(1):31–46, Jan 2010. ISSN 1471-0064. doi: 10.1038/nrg2626. URL <https://doi.org/10.1038/nrg2626>.
- [2] Mohammed Alser, Jeremy Rotman, Dhriti Deshpande, Kodi Taraszka, Huwenbo Shi, Pelin Icer Baykal, Harry Taegyung Yang, Victor Xue, Sergey Knyazev, Benjamin D. Singer, Brunilda Balliu, David Koslicki, Pavel Skums, Alex Zelikovskiy, Can Alkan, Onur Mutlu, and Serghei Mangul. Technology dictates algorithms: recent developments in read alignment. *Genome Biology*, 22(1):249, Aug 2021. ISSN 1474-760X. doi: 10.1186/s13059-021-02443-7. URL <https://doi.org/10.1186/s13059-021-02443-7>.
- [3] Glennis A. Logsdon, Mitchell R. Vollger, and Evan E. Eichler. Long-read human genome sequencing and its applications. *Nature Reviews Genetics*, 21(10):597–614, Oct 2020. ISSN 1471-0064. doi: 10.1038/s41576-020-0236-x. URL <https://doi.org/10.1038/s41576-020-0236-x>.
- [4] Sara Goodwin, John D. McPherson, and W. Richard McCombie. Coming of age: ten years of next-generation sequencing technologies. *Nature Reviews Genetics*, 17(6):333–351, Jun 2016. ISSN 1471-0064. doi: 10.1038/nrg.2016.49. URL <https://doi.org/10.1038/nrg.2016.49>.
- [5] Vivien Marx. Method of the year: long-read sequencing. *Nature Methods*, 20(1):6–11, Jan 2023. ISSN 1548-7105. doi: 10.1038/s41592-022-01730-w. URL <https://doi.org/10.1038/s41592-022-01730-w>.
- [6] Ben Bettisworth, Nikolaos Psonis, Nikos Poulakakis, Pavlos Pavlidis, and Alexandros Stamatakis. Read length dominates phylogenetic placement accuracy of ancient DNA reads. *Mol Biol Evol*, 42(2), February 2025.
- [7] Adrian W. Briggs, Udo Stenzel, Philip L. F. Johnson, Richard E. Green, Janet Kelso, Kay Prüfer, Matthias Meyer, Johannes Krause, Michael T. Ronan, Michael Lachmann, and Svante Pääbo. Patterns of damage in genomic DNA sequences from a Neandertal. *Proceedings of the National Academy of Sciences*, 104(37):14616–14621, 2007. doi: 10.1073/pnas.0704665104. URL <https://www.pnas.org/doi/abs/10.1073/pnas.0704665104>.
- [8] Edo Dotan, Elya Wygoda, Noa Ecker, Michael Alburquerque, Oren Avram, Yonatan Belinkov, and Tal Pupko. BetaAlign: a deep learning approach for multiple sequence alignment. *Bioinformatics*, 41(1):btaf009, 01 2025. ISSN 1367-4811. doi: 10.1093/bioinformatics/btaf009. URL <https://doi.org/10.1093/bioinformatics/btaf009>.
- [9] Aryan Lall and Siddharth Tallur. Deep reinforcement learning-based pairwise DNA sequence alignment method compatible with embedded edge devices. *Scientific Reports*, 13(1):2773, Feb 2023. ISSN 2045-2322. doi: 10.1038/s41598-023-29277-6. URL <https://doi.org/10.1038/s41598-023-29277-6>.
- [10] Pablo Millán Arias, Fatemeh Alipour, Kathleen A. Hill, and Lila Kari. DeLUCS: Deep learning for unsupervised clustering of DNA sequences. *PLOS ONE*, 17(1):1–25, 01 2022. doi: 10.1371/journal.pone.0261531. URL <https://doi.org/10.1371/journal.pone.0261531>.

- [11] Akosua Busia, George Dahl, Clara Fannjiang, David Alexander, Lizzie Dorfman, Ryan Poplin, Cory McLean, Pi-Chuan Chang, and Mark DePristo. A deep learning approach to pattern recognition for short DNA sequences. *bioArxiv*, 2018. URL <https://www.biorxiv.org/content/early/2018/06/22/353474>.
- [12] Akash Shrestha. Read alignment using deep neural networks. *bioArxiv*, 2019. URL <https://mountainscholar.org/items/1a3b3cef-6994-45f3-b9c0-dcddeb1ea5c4>.
- [13] Florian Schroff, Dmitry Kalenichenko, and James Philbin. FaceNet: A unified embedding for face recognition and clustering. In *2015 IEEE Conference on Computer Vision and Pattern Recognition (CVPR)*, page 815–823. IEEE, June 2015. doi: 10.1109/cvpr.2015.7298682. URL <http://dx.doi.org/10.1109/CVPR.2015.7298682>.
- [14] Ting Chen, Simon Kornblith, Mohammad Norouzi, and Geoffrey Hinton. A simple framework for contrastive learning of visual representations. In *Proceedings of the 37th International Conference on Machine Learning, ICML'20*. JMLR.org, 2020.
- [15] Kihyuk Sohn. Improved deep metric learning with multi-class N-pair loss objective. In D. Lee, M. Sugiyama, U. Luxburg, I. Guyon, and R. Garnett, editors, *Advances in Neural Information Processing Systems*, volume 29. Curran Associates, Inc., 2016. URL https://proceedings.neurips.cc/paper_files/paper/2016/file/6b180037abbebea991d8b1232f8a8ca9-Paper.pdf.
- [16] Travis C. Glenn. Field guide to next-generation DNA sequencers. *Molecular Ecology Resources*, 11(5):759–769, 2011. doi: <https://doi.org/10.1111/j.1755-0998.2011.03024.x>. URL <https://onlinelibrary.wiley.com/doi/abs/10.1111/j.1755-0998.2011.03024.x>.
- [17] Prannay Khosla, Piotr Teterwak, Chen Wang, Aaron Sarna, Yonglong Tian, Phillip Isola, Aaron Maschiot, Ce Liu, and Dilip Krishnan. Supervised contrastive learning. In H. Larochelle, M. Ranzato, R. Hadsell, M.F. Balcan, and H. Lin, editors, *Advances in Neural Information Processing Systems*, volume 33, pages 18661–18673. Curran Associates, Inc., 2020. URL https://proceedings.neurips.cc/paper_files/paper/2020/file/d89a66c7c80a29b1bdbab0f2a1a94af8-Paper.pdf.
- [18] Zhuang Liu, Hanzi Mao, Chao-Yuan Wu, Christoph Feichtenhofer, Trevor Darrell, and Saining Xie. A ConvNet for the 2020s. In *Proceedings of the IEEE/CVF Conference on Computer Vision and Pattern Recognition (CVPR)*, pages 11976–11986, June 2022.
- [19] Ting Chen, Ruixiang Zhang, and Geoffrey Hinton. Analog bits: Generating discrete data using diffusion models with self-conditioning, 2023. URL <https://arxiv.org/abs/2208.04202>.
- [20] Alec Radford and Karthik Narasimhan. Improving language understanding by generative pre-training, 2018.
- [21] National Center for Biotechnology Information (NCBI). *Escherichia coli* str. K-12 substr. MG1655, complete genome. https://www.ncbi.nlm.nih.gov/nuccore/NC_000913.3, 2022. URL https://www.ncbi.nlm.nih.gov/nuccore/NC_000913.3. GenBank accession: NC_000913.3.
- [22] Gabriel Renaud, Kristian Hanghøj, Eske Willerslev, and Ludovic Orlando. gargammel: a sequence simulator for ancient DNA. *Bioinformatics*, 33(4):577–579, 11 2016. ISSN 1367-4803. doi: 10.1093/bioinformatics/btw670. URL <https://doi.org/10.1093/bioinformatics/btw670>.
- [23] Weichun Huang, Leping Li, Jason R. Myers, and Gabor T. Marth. ART: a next-generation sequencing read simulator. *Bioinformatics*, 28(4):593–594, 12 2011. ISSN 1367-4803. doi: 10.1093/bioinformatics/btr708. URL <https://doi.org/10.1093/bioinformatics/btr708>.
- [24] Adrien Oliva, Raymond Tobler, Bastien Llamas, and Yassine Souilmi. Additional evaluations show that specific BWA-aln settings still outperform BWA-mem for ancient DNA data alignment. *Ecol Evol*, 11(24):18743–18748, December 2021.

- [25] Ben Langmead, Cole Trapnell, Mihai Pop, and Steven L Salzberg. Ultrafast and memory-efficient alignment of short DNA sequences to the human genome. *Genome Biology*, 10(3):R25, March 2009.
- [26] Adrien Oliva, Raymond Tobler, Alan Cooper, Bastien Llamas, and Yassine Souilmi. Systematic benchmark of ancient DNA read mapping. *Brief Bioinform*, 22(5), September 2021.
- [27] Ryosuke Okuta, Yuya Unno, Daisuke Nishino, Shohei Hido, and Crissman Loomis. CuPy: A NumPy-compatible library for NVIDIA GPU calculations. In *Proceedings of Workshop on Machine Learning Systems (LearningSys) in The Thirty-first Annual Conference on Neural Information Processing Systems (NIPS)*, 2017. URL http://learningsys.org/nips17/assets/papers/paper_16.pdf.
- [28] Leland McInnes, John Healy, and James Melville. UMAP: Uniform manifold approximation and projection for dimension reduction, 2020. URL <https://arxiv.org/abs/1802.03426>.
- [29] Derrick E Wood, Henry Lin, Ami Levy-Moonshine, Rajiswari Swaminathan, Yi-Chien Chang, Brian P Anton, Lais Osmani, Martin Steffen, Simon Kasif, and Steven L Salzberg. Thousands of missed genes found in bacterial genomes and their analysis with COMBREX. *Biol Direct*, 7: 37, October 2012.
- [30] Lingling Shi, Yunfei Guo, Chengliang Dong, John Huddleston, Hui Yang, Xiaolu Han, Aisi Fu, Quan Li, Na Li, Siyi Gong, Katherine E. Lintner, Qiong Ding, Zou Wang, Jiang Hu, Depeng Wang, Feng Wang, Lin Wang, Gholson J. Lyon, Yongtao Guan, Yufeng Shen, Oleg V. Evgrafov, James A. Knowles, Françoise Thibaud-Nissen, Valerie Schneider, Chack-Yung Yu, Libing Zhou, Evan E. Eichler, Kwok-Fai So, and Kai Wang. Long-read sequencing and de novo assembly of a Chinese genome. *Nature Communications*, 7(1):12065, Jun 2016. ISSN 2041-1723. doi: 10.1038/ncomms12065. URL <https://doi.org/10.1038/ncomms12065>.
- [31] Adam Ameer, Huiwen Che, Marcel Martin, Ignas Bunikis, Johan Dahlberg, Ida Höijer, Susana Häggqvist, Francesco Vezzi, Jessica Nordlund, Pall Olason, Lars Feuk, and Ulf Gyllensten. De novo assembly of two swedish genomes reveals missing segments from the human GRCh38 reference and improves variant calling of Population-Scale sequencing data. *Genes (Basel)*, 9(10), October 2018.
- [32] Zhikun Wu, Tong Li, Zehang Jiang, Jingjing Zheng, Yizhou Gu, Yizhi Liu, Yun Liu, and Zhi Xie. Human pangenome analysis of sequences missing from the reference genome reveals their widespread evolutionary, phenotypic, and functional roles. *Nucleic Acids Res*, 52(5):2212–2230, March 2024.
- [33] Torsten Günther and Carl Nettelblad. The presence and impact of reference bias on population genomic studies of prehistoric human populations. *PLoS Genet*, 15(7):e1008302, July 2019.
- [34] Martín Abadi, Ashish Agarwal, Paul Barham, Eugene Brevdo, Zhifeng Chen, Craig Citro, Greg S. Corrado, Andy Davis, Jeffrey Dean, Matthieu Devin, Sanjay Ghemawat, Ian Goodfellow, Andrew Harp, Geoffrey Irving, Michael Isard, Yangqing Jia, Rafal Jozefowicz, Lukasz Kaiser, Manjunath Kudlur, Josh Levenberg, Dandelion Mané, Rajat Monga, Sherry Moore, Derek Murray, Chris Olah, Mike Schuster, Jonathon Shlens, Benoit Steiner, Ilya Sutskever, Kunal Talwar, Paul Tucker, Vincent Vanhoucke, Vijay Vasudevan, Fernanda Viégas, Oriol Vinyals, Pete Warden, Martin Wattenberg, Martin Wicke, Yuan Yu, and Xiaoqiang Zheng. TensorFlow: Large-scale machine learning on heterogeneous systems, 2015. URL <https://www.tensorflow.org/>. Software available from tensorflow.org.
- [35] Heng Li and Richard Durbin. Fast and accurate short read alignment with Burrows-Wheeler transform. *Bioinformatics*, 25(14):1754–1760, May 2009.

A Technical Appendices and Supplementary Material

A.1 Additional position-prediction results

In addition to the mapping scores shown in Table 1, this section provides additional details on the raw accuracy of the position prediction heads before, when the local alignment step is omitted. An

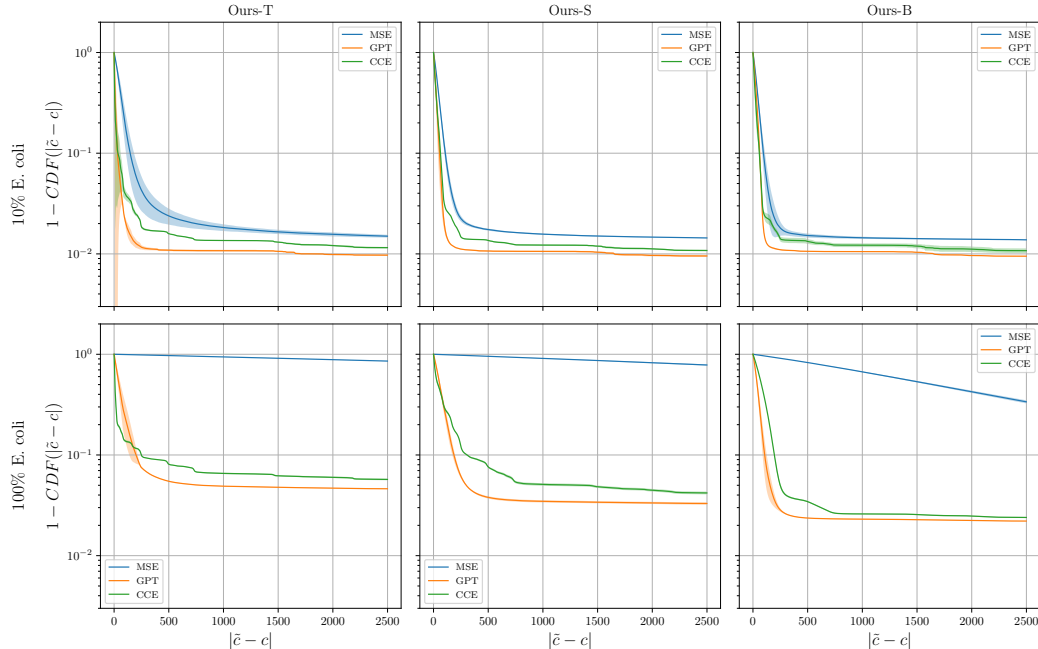


Figure 9: Performance of the different models measured by the quantity empirical CDF of the prediction error. Shown is 1-CDF, lower is better.

effective mapping model assigns many reads close to their true locations. To quantify this, we compute the empirical cumulative distribution function (eCDF) of the absolute prediction error $|\hat{c}(x_i) - c_i|$, representing the fraction of reads mapped within a given distance from their true positions. That is, we compute

$$eCDF(t) = \frac{1}{N} \sum_{i=1}^N \mathbb{1}_{|\hat{c}(x_i) - c_i| < t} \quad (4)$$

In order to amplify differences of importance, we plot $1 - eCDF(t)$ in a logarithmic scale for the runs on 10% and 100% of the *E. coli* genome, for all models, in Figure 9. For each model we made three replicate runs. The lines in the plots are the median, and the shaded region around each represents the minimum and maximum. In many of the plots, the shaded regions are barely visible, reflecting the high reproducibility for the bit-predicting models. We opted to report the full span of our replicates centering on the median, rather than standard deviations, due to the low sample count. This, in turn, was limited due to available computational resources. Figure 10 compares the two bit-prediction models with different sizes of CReadNet trained on the full genome, showing that the more complex models produce embeddings that enable the prediction heads to predict the coordinate more accurately. It also shows that in terms of precision, the GPT model outperforms the base MLP. The post-alignment scores for all runs are shown in Table 2.

A.2 Training setting and hyperparameters

Table 3 shows the hyperparameter settings used for training the models. We used the same optimizer (AdamW) for training the encoder as well as the prediction models. We tried others (LARS, RMSprop, SGD with momentum), but found AdamW to be the most reliable across scenarios.

A.3 Gargammel settings

We use the Briggs [7] damage model. The parameters employed are similar to those cited for Neanderthal DNA in [7]. Our exact choice of parameters to create the aDNA reads with gargammel are listed in Table 4. This is done to try to mimic realistic damage patterns in the simulated reads

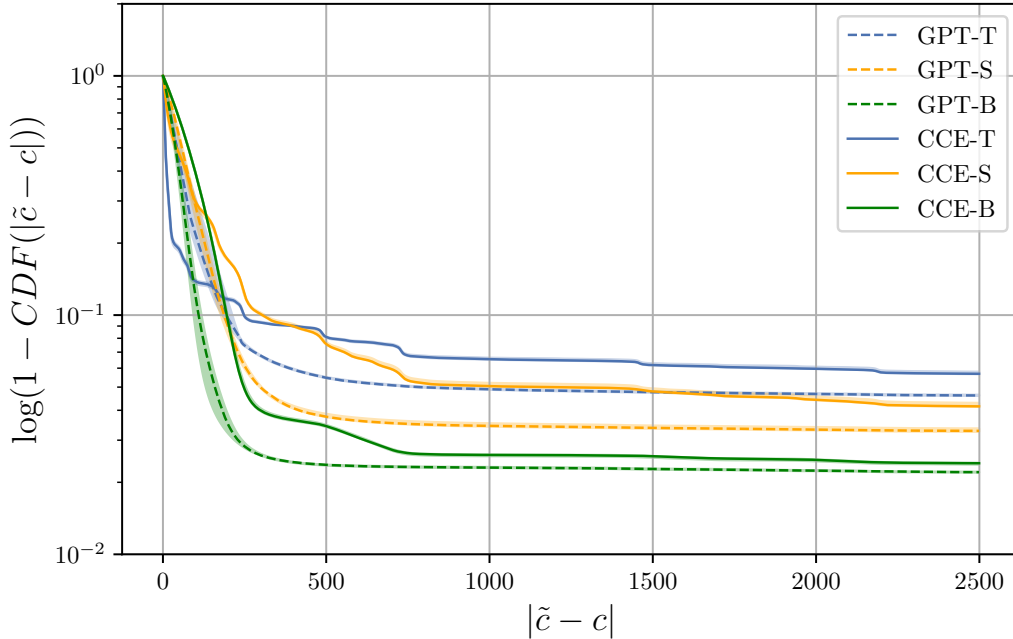


Figure 10: Closer look at the prediction performance on the full *E. coli* with the two bit-prediction models and three different sizes of CReadNet.

Data size	Model	Min	Median	Max
10%	Tiny-MSE	98.36	98.36	98.41
	Tiny-CCE	98.70	98.71	98.73
	Tiny-GPT	98.89	98.90	98.91
	Small-MSE	98.43	98.43	98.44
	Small-CCE	98.78	98.78	98.80
	Small-GPT	98.90	98.91	98.93
	Big-MSE	98.49	98.49	98.50
	Big-CCE	98.77	98.78	98.83
	Big-GPT	98.91	98.92	98.92
100%	Tiny-MSE	14.24	14.40	14.55
	Tiny-CCE	94.09	94.19	94.20
	Tiny-GPT	95.23	95.26	95.27
	Small-MSE	21.03	21.50	22.40
	Small-CCE	95.58	95.72	95.73
	Small-GPT	96.51	96.59	96.62
	Big-MSE	65.59	65.64	66.91
	Big-CCE	97.47	97.47	97.50
	Big-GPT	97.65	97.66	97.67

Table 2: The scores for the replicate runs made, the same as used in reporting the median in Table 1.

using in performance evaluation. The deamination pattern in the reads simulated with gargammel is shown in Figure 11, where we show the frequency for the substitutions $C \rightarrow T$ in the 5' direction and $G \rightarrow A$ in the 3' direction. Comparing this to our aDNA augmentation, where we for the first and last 10 bp increase the substitution rate to 10%, we can conclude that we are using relatively heavy augmentation. There is an inherent point in not simulating reads based on a model identical to the one used for augmentation to show that we can generalize beyond a highly specific noise pattern.

Setting	Value
Optimizer	AdamW, $\beta_1 = 0.9, \beta_2 = 0.999$
Learning rate	0.5e-3
Weight decay	1e-5
LR Schedule	Cosine decay
Warmup	2500 iterations
Initialization	TruncatedNormal(0, 0.05)
Batch size	4096
Epochs 10%/100% <i>E. coli</i>	50 000/15 0000
Epochs prediction head	10 000
Threshold Γ	1 000 (unless otherwise specified)
Positive offset d	50
Flat substitution rate	1%
Temperature τ	0.1

Table 3: Hyperparameter settings used in training both the encoder model and prediction heads.

Read argument	Value
Fragment length (-l)	30
Coverage (-c)	20
Briggs deamination settings	
Nick frequency	0.03
Length of overhanging ends (geometric parameter)	0.4
Probability of deamination of Cs in double-stranded parts	0.01
Probability of deamination of Cs in single-stranded parts	0.7

Table 4: Parameter setting used for generating the aDNA reads with Gargammel.

A.4 Computational resources

The embeddings used in mapping reads from the full *E. coli* genome used 16 A100s 40GB, and was trained for 150 000 iterations, taking approximately 12 hours, and a total of 192 GPUh. This is expensive for a small genome, but continued efforts to improve architecture and optimization strategy could give more reasonable timings. The models trained on 10% used two A100s, and were trained for 50 000 iterations, resulting in 4 GPUh. The models were trained without early stopping, and

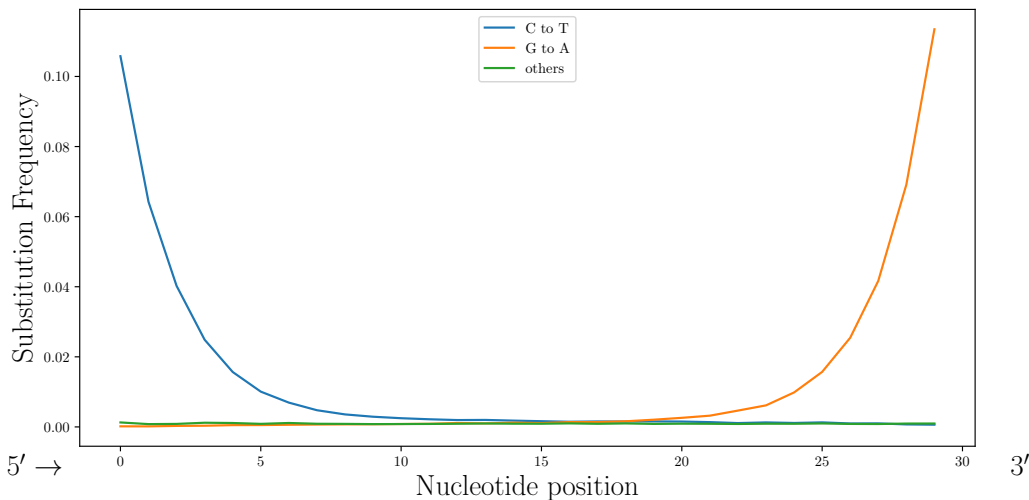


Figure 11: Substitution frequencies of the reads after simulated deamination using the Gargammel read simulator with parameters according to a known damage profile for ancient DNA.

the numbers may thus be a bit larger than they need to be. Training the position prediction task is comparably cheap, being done on one A100, for 10 000 iterations. The most expensive model, the GPT head trained on CReadNet-B, takes 13 minutes in total, and the cheapest, regression on CReadNet-T takes 2.6 minutes. The hardware used for inference with the deep learning models is a single A100 Nvidia GPU. The other aligners (BWA-aln, BWA-mem, bowtie2) are CPU-based implementations, and we used 16 cores of an AMD EPYC 7742 CPU, which is the default number of CPU given per GPU on the cluster used.

The embedding plots in Figures 5 and 6 were trained in the same way as the read mapping models for the 10% case. The experiment shown in Figure 8 was run on an A2000 laptop GPU with 4GB VRAM, for 3000 iterations.

A.5 Software

The code developed for this project was written in Python, using TensorFlow version 2.15 [34]. We used BWA version 0.7.18-r1243-dirty [35] and Bowtie2 version 2.5.4 [25].

In read mapping using Bowtie2, we used the options `-p 16 -very-sensitive`, and for BWA-mem, we used `-k 19 -r 2.5 -t 16`, as recommended in the literature.

A.6 CReadNet Architecture

The description of the encoder in the main text is a bit brief, and in Table 5 we show the full encoder.

Layer		Output Shape
Input		(batch, 30, 4)
Convolution + LN	$S = 1, K = 3, C = 64$, GeLU	(batch, 30, 64)
Stage 1 ResBlocks	$B = 3, C = 64$	(batch, 30, 64)
AveragePooling	$S = 2, K = 2$	(batch, 15, 64)
Convolution	$K = 3, C = 128$, GeLU	(batch, 15, 128)
Stage 2 ResBlocks	$B = 3, C = 128$	(batch, 15, 128)
AveragePooling	$S = 2, K = 2$	(batch, 8, 128)
Convolution	$K = 3, C = 256$, GeLU	(batch, 8, 256)
Stage 3 ResBlocks	$B = 9, C = 256$	(batch, 8, 128)
AveragePooling	$S = 2, K = 2$	(batch, 4, 256)
Convolution	$K = 3, C = 512$, GeLU	(batch, 4, 512)
Stage 3 ResBlocks	$B = 3, C = 512$	(batch, 15, 512)
GlobalAveragePooling		(batch, 4, 512)
Representation (dense)	units= 512, L2 norm, GeLU	(batch, 512)
Embedding (dense)	units = 256, L2 Norm	(batch, 256)

Table 5: Architecture of CReadNet-T. Here, K denotes kernel size, C number of convolution filters, B the number of residual blocks in each stage. To scale the model, the number of blocks in stage 3 is increased to 27 (giving CReadNet-S), and the base filter count is increased from 64 to 96 (CReadNet-B).

A.7 GPT-bit prediction architecture

This section provides a more detailed description of the GPT model architecture than what is presented in the main paper. The GPT model takes as input the 512-dimensional output Y of the three-layer MLP. This output is split into 8 tokens of size 64, denoted as

$$Y = [Y_1, \dots, Y_8], \quad Y_i \in \mathbb{R}^{64}.$$

The model also receives a sequence of targets representing the bit-wise representation of the coordinates

$$T = [t_1, t_2, \dots, t_{N_b}],$$

and takes all but the last bit $T_- = [t_1, t_2, \dots, t_{N_b-1}]$, and tries to sequentially predict the next bit at each step. For the bit tokens, we use a trainable embedding $E \in \mathbb{R}^{2 \times 64}$, and append it to the MLP tokens, and apply a trainable positional encoding E_{pos} to get the combined input

$$y = [Y_1, \dots, Y_8, t_1 E, t_2 E, \dots, t_{N_b-1} E] + E_{pos}.$$

This input is processed by a Transformer decoder block, with multi-head self-attention (MSA), layer normalization (LN), and a 2-layer feed forward network (FF), finishing with a dense layer with b units as:

$$\begin{aligned} a &= \text{LN}(\text{MSA}(y) + y), \\ y &= \text{LN}(\text{FF}(a) + a), \\ Z &= \text{softmax}(\text{Dense}(y)), \end{aligned}$$

The MSA has a *causal mask* that prevents backward information flow across the bit-tokens, but allows full attention over the MLP tokens. The output Z has dimensions $\mathbb{R}^{(8+N_b-1, b)}$, and during training, the first 7 tokens are discarded, and the remaining ones are trained to predict the true bit representation T of the coordinates by minimizing the categorical cross entropy loss. The FF network inside the GPT model has two layers, with 256 and 64 units, respectively, with GeLU activation between them. As stated in the main text, we use 2 heads in the MSA, and the final dense layer before the softmax has b units, bringing the output dimension to $\mathbb{R}^{(8+N_b, b)}$, in this case. Thus, the output is the shifted sequence $Z = [\tilde{Y}_2, \dots, \tilde{Y}_8, \tilde{t}_1, \dots, \tilde{t}_{N_b}]$, and we can extract the predicted bit sequence $[\tilde{t}_1, \dots, \tilde{t}_{N_b}]$ to use as the final prediction of the bit-wise representation.